Polymer Photocatalysts with Side Chain Induced Planarity for Increased Activity for Sacrificial Hydrogen Production from Water

Richard J. Lyons, Ying Yang, Ewan McQueen, Liang Luo, Andrew I. Cooper, Martijn A. Zwijnenburg,* and Reiner Sebastian Sprick*

Conjugated polymers are promising materials for photocatalytic hydrogen evolution. However, most reported materials are not solution-processible, limiting their potential for large-scale application, for example as solution cast films. Flexible side-chains are commonly introduced to provide solubility, but these often impart unfavorable properties, such as hydrophobicity, which lowers photocatalytic activity. Here, computational predictions are employed to aid in the design of chloroform soluble polymer photocatalysts that show increased planarity through favorable intramolecular interactions. Using this approach, three conjugated polymer photocatalysts with identical poly(benzene-dibenzo[b,d]thiophene sulfone) backbones but different solubilizing side-chains on the benzene-ring are explored, i.e., tri(ethylene glycol), n-decyloxy, and n-dodecyl. These side-chain variations significantly alterr the properties of the polymers, specifically energy levels, optical gap, and wettability. The hydrophobic n-decyloxy functionalized polymer has a sacrificial hydrogen evolution rate of 17.0 µmol h^{-1} in suspension, while the hydrophilic tri(ethylene glycol) functionalized polymer is almost three times more active (45.4 µmol h^{-1}). Conversely, no hydrogen evolution is observed for the purely alkyl side-chain (n-dodecyl) containing polymer due to the side-chain induced torsion of the backbone. A thin-film of the most active polymer exhibits a promising area-normalized sacrificial hydrogen evolution rate of 7.4 ± 0.3 mmol h^{-1} m^{-2} under visible light irradiation.

1. Introduction

The conversion of solar energy into renewable fuels such as hydrogen by water splitting has attracted significant attention.[1,2] Since the work of Fujishima and Honda in 1972 on the photoelectrochemical evolution of hydrogen from water, much research has been performed to develop photocatalysts for water splitting.[3] Studies have focused on inorganic materials for the most part[4–6] but more recently, organic polymer photocatalysts have garnered interest due to their relatively simple synthetic tunability.[1] Since the early work by Yanagida et al. in 1985 on the use of poly(p-phenylene) as photocatalysts for sacrificial hydrogen evolution from water,[7] several families of polymer photocatalysts have been explored for water splitting, including carbon nitrides,[8,9] covalent triazine-based frameworks,[10–12] conjugated microporous polymers (CMPs),[13] covalent organic frameworks,[14–17] and linear polymers.[18–23] More recently other classes of organic photocatalysts, such as polymer gels,[24] hydrogen bonded organic frameworks,[25] conjugated oligomers,[26] and molecular photocatalysts[27–30] have also been explored for hydrogen evolution. However, due to restricted processability of many of these materials, generally stemming from poor solubility in organic solvents, conjugated polymers decorated with solubilizing side chains have attracted interest due to their relative ease of processing. Exploitation of this solubility has resulted in significant improvement in photocatalytic performance through the preparation of systems, such as

R. J. Lyons, Y. Yang, L. Luo, A. I. Cooper
Department of Chemistry and Materials Innovation Factory
University of Liverpool
Liverpool L7 3NY, UK

The ORCID identification number(s) for the author(s) of this article can be found under https://doi.org/10.1002/aenm.202303680

E. McQueen, R. S. Sprick
Department of Pure and Applied Chemistry
University of Strathclyde
Glasgow G1 1XL, UK
E-mail: sebastian.sprick@strath.ac.uk

M. A. Zwijnenburg
Department of Chemistry
University College London
London WC1H 0AJ, UK
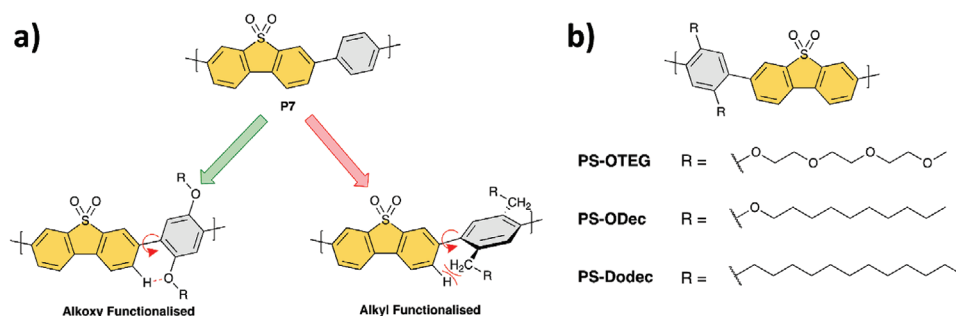E-mail: m.zwijnenburg@ucl.ac.uk

Figure 1. a) Impact of the alkoxy and alkyl side chain on the dihedral angle of the PS polymers; b) Structures of the repeat unit of the PS-OTEG, PS-ODec, and PS-Dodec polymers.

polymer dots,[31–34] nanoprecipitates,[35] heterojunctions,[38–41] and thin-films.[22,23,36]

Although some promising solution-processable polymer photocatalysts have been reported,[22,35,37] they often have significantly poorer photocatalytic activity for sacrificial hydrogen evolution compared to other insoluble materials,[38–41] and, in some cases, compared to insoluble analogs with near identical backbone architecture.[22,23] Often, this low photocatalytic performance was ascribed to poor wettability resulting from hydrophobic alkyl side chains. These issues have been to some extent circumvented by variation of the length or composition of the side chains, which can improve the photocatalyst's affinity for water or dielectric properties.[22,42–44] Many of the reported solution processable photocatalysts possess side-chains attached to monomers such as functionalized carbazoles,[23,35] benzodithiophenes,[42,45] cyclopentadithiophene,[46] and indacenodithiophene.[22,43,47] Side chains appended to these monomers may have some impact on the polymer's opto-electronic properties through inductive, mesomeric and/or steric effects and it is therefore important to consider the consequences of side chain engineering on the optoelectronic properties and the resulting photocatalytic activity. In particular, steric repulsion arising from solubilizing side chains can result in heavily restricted rotation about the single bonds between adjacent monomers, distorting the backbone from planarity. This twisting will prevent or limit the overlap of adjacent p-orbitals and will confine conjugation within individual monomers, resulting in increased localization of excitons and charge carriers. Steric effects are not unique to conjugated materials with side-chains: polymers without side-chains will still be subject to steric effects, but the energy barriers to allow rotation about the backbone of polymers without side chains will be significantly lower.[48] While backbone twisting could be circumvented through the formation of ladder-type conjugated polymers, these polymers will have multiple covalent bonds between adjacent monomer units, which act to completely restrict rotation about the backbone, permanently altering the overall architecture compared to their less rotationally restricted, nonladder analogues.[21,49] Ladder polymers also tend to have low solubilities. The use of side chains that promote planarization, similarly to ladder-type polymers, through non-covalent interactions could be used to create polymers that combine the benefits of both solution processability and backbone planarity.

Here, we show how subtle variations in side-chain composition can be exploited to create significant changes in the optoelectronic properties of polymers by improving donor–acceptor character and backbone planarity through non-conventional hydrogen bonds and electronic (inductive/mesomeric) effects, resulting in significant changes to the photocatalytic activity. Using P7, a co-polymer of dibenzo[b,d]thiophene sulfone and phenylene (**Figure 1a**), as a starting point we used density functional theory (DFT) and (time-dependent) density functional theory ((TD)-DFT) in the design of solution processable analogues of P7, while considering carefully the impact intramolecular interactions from the side-chains have on the opto-electronic properties of the bulk materials (Figure 1a). We then expanded upon the theoretical study and synthesized three solution processable polymers with minimal variation in side-chain composition. The polymers synthesized contained either n-dodecyl (PS-Dodec), n-decoxy (PS-ODec), or tri(ethylene glycol) (PS-OTEG) solubilizing side-chains on the benzene co-monomer (Figure 1b). Using the theoretical study and the optical results, we then studied the photocatalytic performance of the materials and considered how the side-chains impacted the sacrificial photocatalytic hydrogen evolution performance in suspension. Finally, we studied the most active polymer, PS-OTEG, as a thin-film photocatalyst, which showed a promising area-normalized hydrogen evolution rate of 7.35 mmol h^{-1} m^{-2} and an external quantum efficiency of 5.3% at 420 nm in suspension.

2. Results and Discussion

2.1. Computational Modelling and Energy Levels

First, we performed a conformer search for models of phenylene and dibenzo[b,d]thiophene sulfone oligomers in the form of (AB)$_2$ decorated with a variety of alkyl and alkoxy side-chains using the GFN2-xTB tight-binding DFT method,[50] followed by a subsequent reoptimization of low energy conformers by means of DFT (B3LYP+D4).[51–55] Subsequently TD-DFT was used to predict the optical gap of the DFT optimized oligomers, while the ionization potential (IP) and electron affinity (EA) were predicted following a previously developed recipe based on ΔDFT calculations in combination with an implicit solvation model to describe the water mixture the polymer particles are dispersed in during photocatalysis.[56,57] For the oligomers modelled we systematically varied the length and composition of the side chains
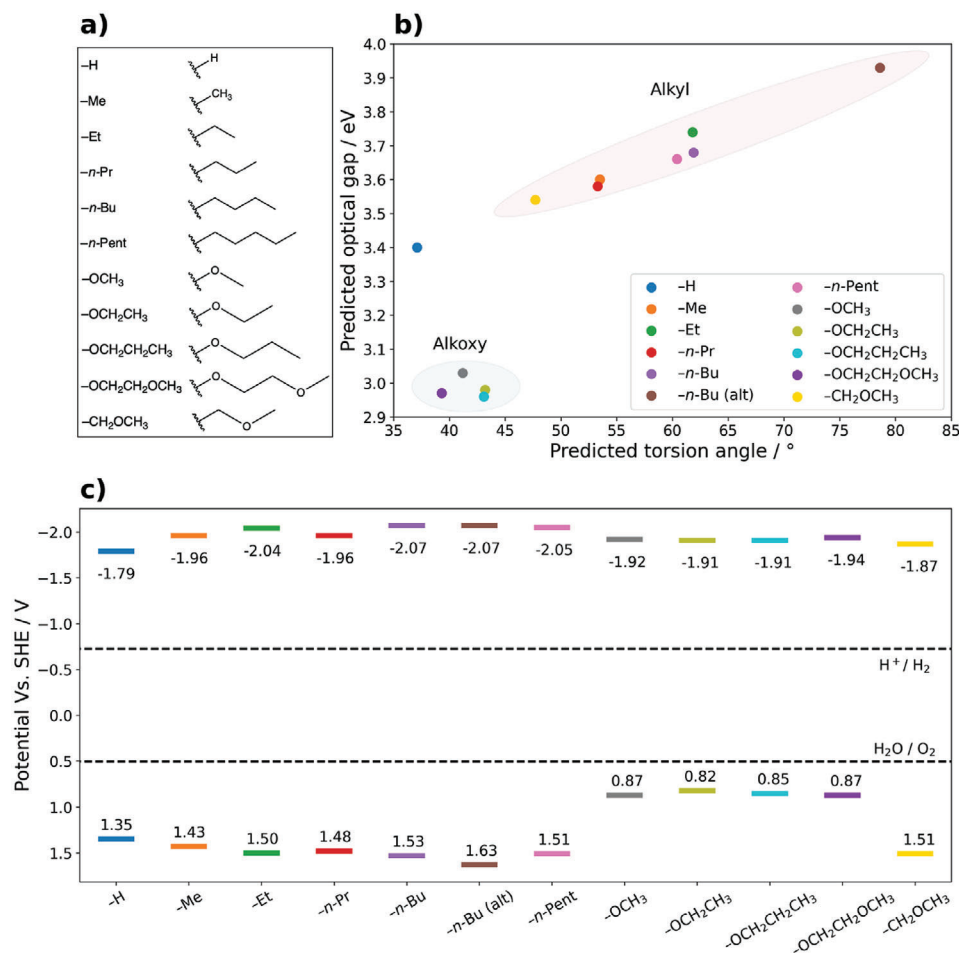
2303680 (2 of 10)

**ADVANCED
SCIENCE NEWS**

www.advancedsciencenews.com

**ADVANCED
ENERGY
MATERIALS**

www.advenergymat.de

Figure 2. a) The structures of the side-chains attached to the oligomers modeled in the theoretical study b) the correlation between the predicted average torsion angle and the predicted optical gaps for alkyl and alkoxy functionalized oligomers; c) Predicted ionization potential and electron affinities of oligomers along with energy levels of water oxidation and proton reduction at pH = 12.3. N.B. n-Bu (alt) refers to an alternative low energy conformer.

to study how they impacted the conformation and optoelectronic properties of the oligomers. As the conformer search became increasingly more computationally expensive with increasing side chain lengths modelled, it became necessary to limit the side-chain lengths decorating the models to those specified in **Figure** 2a.

The gas phase conformer searches for the different oligomers found that structures bearing different side-chains were found to adopt quite different conformers. In the case of the oligomers with alkoxy side-chains, the structures of the lowest-energy conformers suggested the formation of weak nonconventional hydrogen bonds between the aryl-alkyl oxygen on the alkoxy side chains with the *ortho/para* hydrogens in the dibenzo[*b,d*]thiophene sulfone unit (Figure 1a). This was indicated by the interatomic distance between the oxygen of the alkoxy and the hydrogen atom (in the range of 240–255 pm) being smaller than the sum of their individual Van der Waals radii ($H = 120$ pm and $O = 152$ pm),[58] which suggests an attractive interaction between them. These nonconventional hydrogen bonds together with the reduced steric repulsion afforded by the substitution of methylene for the ether linkage stabilize a relatively planar polymer backbone for oligomers pos-

sessing these alkoxy side-chains with a torsion angle between the adjacent monomers of on average ca. 42° (Figure 2b). The lowest predicted torsion angle for a functionalized oligomer was for the oligomer containing an ethylene glycol side-chain ($-OCH_2CH_2OCH_3$), which was found to be 39.3°. This torsion angle was close to the angle predicted for the unfunctionalized oligomer ($-H$) which was predicted to be 37.1°, suggesting that the C$-$H$\cdots$O interaction may not be sufficiently strong to compensate for the steric effects of the presence of a side-chain. Whereas for the alkyl functionalized oligomers, the adjacent monomers are mostly out of plane with a much larger spread of angles compared to the alkoxy functionalized oligomers (Figure 2b). The larger torsion angles are a consequence of the steric repulsion between the *ortho/para* protons of the dibenzo[*b,d*]thiophene sulfone unit and the first methylene (or methyl) group of the alkyl side-chain on the adjacent phenylene-type unit (Figure 1a). There was no clear trend between side-chain length and torsion angle observed, but unexpectedly, oligomers with alkyl side-chains with an even number of carbons ($-Et$, $-n$-Bu) were found to have larger torsion angles than those with an odd number of carbons ($-Me$, $-n$-Pr, $-n$-Pent).

2303680 (3 of 10)

The effect of side chains on the oligomer structures predicted here is supported by previous work that suggested that polymers formed using six-membered aromatic scaffolds, such as our oligomers, will possess significant steric interactions between adjacent rings, in which the substitution of the hydrogen *ortho* to the σ-bond formed between adjacent monomers for another functional group will always act to decrease the coplanarity between adjacent monomers.[48] Furthermore, Bryce and co-workers observed a similar reduction in the predicted torsion angle as predicted here when substituting alkyl with alkoxy side chains for oligomers made from carbazole monomers linked by 2,4-subtituted phenylenes for organic light emitting diodes.[59] There have also been reports elsewhere of noncovalent intramolecular interactions utilized to assert conformational control in order to allow for the formation of more planar backbone structures, however, these systems often possess less sterically demanding environments, such as the use of thiophene rather than phenylene,[60] or stronger intramolecular interactions, such as conventional H-bonds and coordination bonds.[61]

The oligomers with alkoxy and alkyl side chains were predicted to not only have different structures but also to differ in their optoelectronic properties, most notably in their optical gap, the lowest excitation energy, and the predicted onset of light absorption. The optical gaps of the oligomers with alkoxy side-chains were predicted to be significantly smaller than those of the oligomers with alkyl side chains (Figure 2b). Furthermore, for the alkyl functionalized oligomers, there was a direct trend between optical gap and torsion angle, highlighting the impact of backbone torsion on the opto-electronic properties. Naïvely, it would be tempting to relate the smaller optical gap of the oligomers with alkoxy side-chains to their more planar structure, constrained by the non-conventional hydrogen bonds, and the improved conjugation afforded by greater co-planarity. This explanation, however, is unlikely to be the whole story, since the oligomers with alkoxy side-chains were also predicted to have smaller optical gaps than the oligomer without side chains (—H), which, as discussed above, possesses yet a more planar conformation than their alkoxy analogues. A significant contribution to the reduction of the optical gap most likely comes from the occupied orbitals moving up in energy, becoming shallower, because of mesomeric electron donation by the electron rich alkoxy oxygen of the side chain into the conjugated backbone, thus increasing the donor character of the phenylene-type unit. This is apparent from the difference in IP between the oligomers with alkoxy side-chains and those with alkyl side chains or no side chain (Figure 2c). Based on the discussion above, one might expect that alkyl functionalization could promote a slight red-shift compared to oligomers without side chains (i.e., —H) as alkyl side-chains weakly donate electron density via induction, thus improving the donor character of the phenylene-type unit. However, this electron donating effect is more than negated by the twisting in the backbone induced by the alkyl side chains. Even if the more planar conformer adopted by the alkoxyl functionalized oligomers is not directly the origin of the reduction in the optical gap for these systems, the fact that the hydrogen bonds and reduced steric repulsion help prevent the twisting observed in alkyl functionalized oligomers means that the hydrogen bonds and reduced steric repulsion are in fact essential to achieve these smaller optical gaps.

As mentioned above, the introduction of side chains is predicted to change both the structure and optical properties as well as the oligomers' electronic properties. Generally, the EA of the oligomers was relatively insensitive to the introduction of side chains, being slightly shallower for the oligomers with alkyl side chains relative to those without or with alkoxy side-chains, which is most likely due to the twisting of the backbone and the reduced conjugation in the former. There is, however, a more dramatic change predicted for the IPs. The IP of the oligomers with alkyl side chains is predicted to be slightly deeper than that of the oligomer without side-chains, again likely due to side chain induced torsion and the reduced conjugation. The IP of the oligomers with alkoxy side-chains is predicted to be 0.4–0.5 V shallower than the oligomers without side chains. As discussed above, this is mostly likely the result of the mesomeric electron donating effect of the alkoxy oxygen. However, even while the IP of the oligomers with alkoxy side chains is predicted to be shallower, these oligomers should still have sufficient driving force to oxidize water and sacrificial donors, such as triethylamine. Finally, it also likely that intrachain exciton and charge transport will be faster in the less twisted oligomers possessing alkoxy side-chains as the more planar structure will result in longer effective conjugation lengths by virtue of the improved overlap between π-orbitals of adjacent monomers.[62] Conversely, backbone twisting will minimize or prevent the overlap of adjacent π-orbitals and will stunt the effective conjugation.[62] Bryce and co-workers observed, as discussed above, a similar reduction in the predicted torsion angle when substituting alkyl with alkoxy side-chains for oligomers made from carbazole monomers linked by 2,4-subtitued phenylenes for organic light emitting diodes, as well as a similar upshift in the IP values, in their case as experimentally extracted from CV, and a red-shift in the experimental optical gap.[59] However, the experimentally observed red-shift for those materials was much smaller than that predicted here for the co-polymers of dibenzo[*b,d*]thiophene sulfone and functionalized benzene.

For the following sections, we used these computational results for the oligomer models possessing the longest side-chains to represent the polymers synthesized since they were the most comparable: that is, *n*-pentyl was used to represent *n*-dodecyl in PS-Dodec, *n*-propoxy to represent *n*-decoxy in PS-ODec, and —OCH$_2$CH$_2$OCH$_3$ to represent tri(ethylene glycol) in PS-OTEG. P7 is represented by the oligomer without side-chains (-H).

2.2. Synthesis and Characterization

Based on our theoretical predictions, we synthesized three polymers, PS-Dodec, PS-ODec, and PS-OTEG, and investigated their optical properties. The three conjugated polymer photocatalysts (Figure 1b) were synthesized by Pd(0) catalyzed Suzuki-Miyaura-type polycondensation from 3,7-bis(4,4,5,5-tetramethyl-1,3,2-dioxaborolan-2-yl)dibenzo[*b,d*]thiophene sulfone and 1,4-dibromo-2,5-bis(2-(2-(2-methoxyethoxy)ethoxy)ethoxy)benzene, 1,4-dibromo-2,5-bis(decyloxy)benzene, or 1,4-didodecyl-2,5-diiodobenzene. PS-OTEG and PS-ODec were both obtained as green powders while PS-Dodec was a light brown powder; all were soluble in chloroform (for full synthetic details see Supporting Information). The ^{1}H{^{13}C} NMR spectra of the polymers

**ADVANCED
SCIENCE NEWS**

www.advancedsciencenews.com
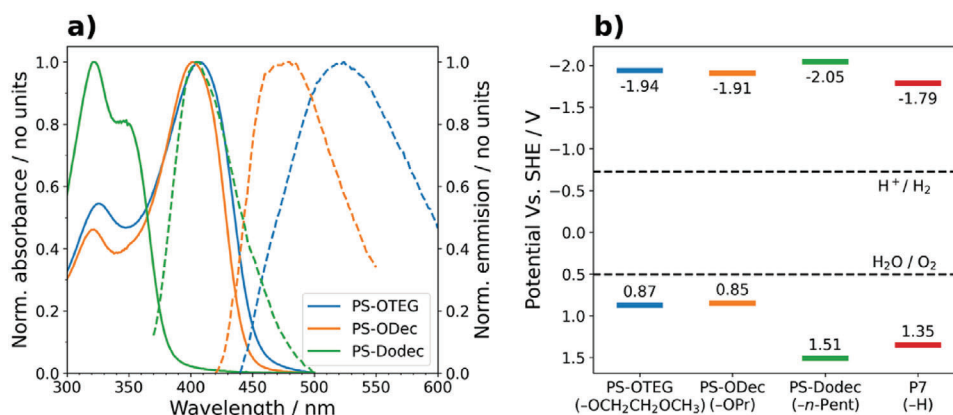
**ADVANCED
ENERGY
MATERIALS**

www.advenergymat.de

Figure 3. a) Normalized UV–vis and photoluminescence spectra of PS-OTEG, PS-ODec, and PS-Dodec as thin-films on glass substrates spin coated from chloroform solutions; b) Predicted ionization potentials and electron affinities of analogous oligomers along with energy levels of water oxidation and proton reduction at pH = 12.3.

(Figure S6, Supporting Information) showed the expected peaks associated with aromatic protons (8.40–7.30 ppm), PEG protons (4.50–3.00 ppm), and alkyl protons (2.00–0.80 ppm). Powder X-ray diffraction (PXRD) patterns of the as-prepared polymers show that all three polymers show limited long-range order (Figure S7, Supporting Information). The Fourier transform infrared (FT-IR) spectroscopy (Figure S8, Supporting Information) of all polymers showed the characteristic asymmetric stretching vibrations of the sulfone group at around 1300 and 1155 cm^{-1}, and peaks at around 3055 and 2866 cm^{-1} which correspond to aromatic and aliphatic C–H stretches, respectively. For PS-OTEG and PS-ODec, a peak was observed at around 1210 cm^{-1} which has been attributed to the aryl-alkyl C-O stretch. Thermogravimetric analysis (TGA) showed good thermal stability under air, with decomposition temperatures (determined at 5 wt% lost) of 321, 365, and 294 °C for PS-OTEG, PS-ODec, PS-Dodec, respectively (Figure S9, Supporting Information).

2.3. UV–vis Absorption and Photoluminescence Spectra

First, we studied the UV–vis absorption and steady-state fluorescence spectra of the soluble polymers as thin-films on glass substrates (**Figure 3**a) and as dilute solutions in chloroform (**Table 1**). As predicted, we found that the UV–vis absorption spectra of PS-OTEG and PS-ODec were similar, with PS-OTEG being

slightly red-shifted compared to PS-ODec as thin films, but as solutions (Figure S11, Supporting Information)—or in the solid state (Figure S13, Supporting Information), discussed in more detail below—they were found to have almost identical optical gaps (Table 1). However, all the spectra for PS-Dodec in solution and as a thin-film showed significant blue-shifting compared to the spectra of PS-OTEG and PS-ODec (Figure 3a and Figure S11, Supporting Information). Similarly, the photoluminescence spectra of PS-Dodec showed a similar blue-shift compared to those of PS-ODec and PS-OTEG (Figures S16–S21, Supporting Information). While the thin-film absorption spectra of PS-ODec and PS-OTEG are similar, the photoluminescence spectra of thin-film of PS-OTEG shows a slight red-shift in emission compared to the PS-ODec film (Figure 3a). Similar red-shifting of the photoluminescence spectra have also been observed in other materials in which there has been a substitution of alkyl for oligo(ethylene glycol) side chains,[42,43] and is a likely consequence of the closer intermolecular packing afforded by oligo(ethylene glycol) side chains compared with alkyl side-chains,[63,64] which is expected to alter the intermolecular interactions which results in the observed emission at longer wavelengths. The values for the optical gap determined experimentally from the absorption onsets of the thin-films of PS-OTEG and PS-ODec were determined to be 2.74 and 2.80 eV, respectively. These values are close to the predicted optical gap values for oligomer models for PS-OTEG and PS-ODec, which were found to be 2.97 and 2.96, respectively. While

Table 1. Optical properties for thin-films and solutions of PS polymers.

Polymer	In CHCl$_3$ solution				Thin film				Solid state
	λ_{max} [a) [nm]	λ_{onset} [b) [nm]	λ_{em} [a,c) [nm]	E_{opt} [d) [eV]	λ_{max} [a) [nm]	λ_{onset} [b) [nm]	λ_{em} [c) [nm]	E_{opt} [d) [eV]	E_{opt} [e) [eV]
PS-OTEG	406	441	462 (482)	2.81	407	452	518	2.74	2.61
PS-Odec	400	440	456	2.81	401	443	480	2.80	2.60
PS-Dodec	317 (343)	375	394	3.31	322 (348)	380	405	3.26	3.00
P7 (lit. 19)	–	–	–	–	–	–	–	–	2.70[b)

a) Values in parentheses correspond to low energy shoulders; b) Determined from the tangent to the absorbance onset; c) The photoluminescence emission maxima excited at the λ_{max} of an excitation scan (Figures S13–S18, Supporting Information); d) Determined from the absorption onset of spin coated thin-films; e) Determined using Tauc plots of diffuse reflection spectra of powder in the solid state.

both experiment and calculations agree on the fact that the optical gap of PS-Dodec is blue-shifted relative to that of PS-OTEG and PS-ODec, there is a larger discrepancy between the experimental and predicted values for optical gap, which were 3.26 and 3.66 eV, respectively. The larger difference between the predicted and experimental values of PS-Dodec could arise from intermolecular interactions between polymer chains in a condensed state which were not accounted for in the gas phase theoretical models. The observed blue-shift of the optical gap of PS-Dodec, relative to that of PS-OTEG and PS-ODec, is similar to that observed experimentally in oligomers made previously from carbazole monomers linked by 2,4-subtitued phenyls.[19]

To allow for greater comparison with the insoluble P7, we also analyzed the soluble polymers as powders by diffuse reflectance spectroscopy (Figure S13, Supporting Information) and extracted the optical gaps from Tauc plots (Table 1, Figure S14, Supporting Information). The results followed the trend predicted by our (TD-)DFT calculations with a slight redshift of the optical gaps of PS-ODec and PS-OTEG compared to that of P7 and a blueshift of the PS-Dodec optical gap (Table 1). We also noted the similarity in the solid-state optical gap of PS-OTEG and PS-ODec, discussed above.

2.4. Lifetime of the Excited State

We used time-correlated single photon counting (TCSPC) to study the lifetime of the excited state of the polymers to better understand how the excited state dynamics are impacted by side-chain variation. These TCSPC experiments were performed for the polymers as suspensions in the photocatalytic reaction mixture (a 1:1:1 mixture of water/triethylamine (TEA)/methanol (MeOH)) at 375 nm excitation (Figures S21–S23 and Table S3, Supporting Information). The estimated excited state lifetimes of PS-OTEG and PS-ODec were estimated to be 0.896 and 0.875 ns, respectively. PS-Dodec was found to have a notably shorter average excited state lifetime of 0.404 ns. Based on our theoretical results, we expect this shortened excited state lifetime observed for PS-Dodec, compared to the alkoxy functionalized polymers, to be a direct consequence of backbone twisting which results in localization of exited-states and faster electron-hole recombination.

2.5. Fluorene-Phenyl Polymers

To compare the observations of the opto-electronic properties of P7, PS-Dodec, and PS-ODec, we synthesized fully chloroform-soluble analogues in the form of fluorene-phenyl co-polymers. All these polymers contained *n*-dodecyl side chains on the bridge-head of the fluorene unit to guarantee solubility of the polymer. The difference between the polymers was from the side-chains at the 1 and 4 positions of the phenylene-type monomer, which were either —H, —*n*-decoxy, or —*n*-dodecyl, these polymers were denoted FP-Dodec, FP-Dodec-ODec, and FP-Dodec-Dodec, respectively. The optical behavior of these polymers was similar those seen for PS-ODec/PS-OTEG and PS-Dodec, with a significant blue shift seen in the absorbance spectrum of FP-Dodec-Dodec compared to that of PS-ODec/PS-OTEG. FP-Dodec, showed sim-

ilar optical properties to the alkyl functionalized polymer, FP-Dodec-ODec. This observation could be due to reduced planarity or poorer donor–acceptor type behavior in FP-Dodec-ODec compared to PS-ODec/PS-OTEG (see Supporting Information for full details of synthesis and analysis). The as-prepared polymers showed no activity for hydrogen evolution and were not studied further.

2.6. Photocatalytic Hydrogen Evolution Experiments

An initial screening of sacrificial conditions for hydrogen evolution was performed to determine the optimum conditions to study the kinetics (see Supporting Information for details and results). Based on this screen and for comparability with previous studies within our group, a 1:1:1 water/MeOH/TEA mixture was chosen to study the kinetic hydrogen evolution of the polymers as powders in suspension.[18,19,22,23,25,40] Following the screening, kinetic hydrogen evolution experiments were performed using visible light illumination ($\lambda \geq 420$ nm, 300 W Xe light source) of polymer suspensions in a 1:1:1 mixture of water/MeOH/TEA with the rates calculated by a linear regression. The results and other relevant data are provided in **Table 2**.

Unsurprisingly no hydrogen was observed for PS-Dodec under visible light illumination ($\lambda \geq 420$ nm). As the absorption onset of PS-Dodec was estimated to be 413 nm for the solid sample it was therefore not possible for photoexcitation to occur when using vissible light. However, the predicted IP and EA (Figure 3b) for PS-Dodec suggested appropriate alignment to drive sacrificial hydrogen evolution, if photoexcitation did occur. We thus repeated the photocatalytic experiment under broadband illumination ($\lambda \geq 295$ nm), during which hydrogen indeed evolved at a steady rate of 60 µmol h^{-1} g^{-1}. This confirmed that PS-Dodec can produce hydrogen under sacrificial conditions provided photoexcitation occurs. However, the rate was significantly lower than both PS-ODec and PS-OTEG under visible light illumination (Table 2 and **Figure 4a**). This rate was also considerably lower than the rate reported for P7 under similar conditions, which was reported as 1492 µmol h^{-1} g^{-1}. The poor photocatalytic performance of PS-Dodec, even under broadband irradiation that includes UV light, is likely due to a combination of factors, such as the larger optical gap providing poor light harvesting capabilities, a relatively short excited-state lifetime, and poor charge mobility due to backbone twisting. It was expected that the hydrophobicity, larger particle size and poor dispersibility in the reaction mixture for PS-Dodec (Table 2) would also contribute to the poor photocatalytic performance. However, the impact of these factors is unlikely to contribute significantly when compared to the effect the opto-electronic properties had on the photocatalytic performance of PS-Dodec. Although similar breaks in conjugation have been demonstrated in other linear polymers and CMPs through 1,3- or *meta*-coupling between monomer units, for these co-polymers the effective conjugation length can, typically, extend across 2 or 3 monomer units.[20,65,66] *Meta*-coupling causes breaks in conjugation through the polymers' backbone architecture; this is a different effect to that observed here, where the break in conjugation for PS-Dodec is purely the consequence of steric repulsions arising from the side-chains. A similar observation was previously seen by Aitchison et al. in oligomer photocatalysts.[26]

**ADVANCED
SCIENCE NEWS**

www.advancedsciencenews.com

**ADVANCED
ENERGY
MATERIALS**

www.advenergymat.de

Table 2. Absolute sacrificial photocatalytic HERs, mass normalized sacrificial photocatalytic HERs, residual palladium content, fluorescence lifetimes, particle size, and transmittance of the PS polymers.

Polymer	HER[a] [μmol h⁻¹]	HER[a,b] [μmol h⁻¹ g⁻¹]	Pd[c] [ppm]	Particle size[d] [μm]	Transmittance[e] [%]	Contact angle[f] [°]
PS-OTEG	45.4 ± 0.9	1817 ± 34	5200	11.6	7.0	61.9 ± 0.9
PS-Odec	17.0 ± 0.1	680 ± 4	1300	13.4	33.3	103.9 ± 2.2
PS-Dodec	0[g]	0[g]	1630	30.4	47.3	109.5 ± 3.6
P7 (lit. 18)	37.3 ± 0.8	1492 ± 32	3800	–	–	67 ± 1.7

[a] Photocatalytic hydrogen evolution rates of the polymer photocatalysts determined in 1:1:1 TEA/MeOH/water at concentration of 1.1 mg mL⁻¹ in 22.5 mL; [b] HER normalized to mass of photocatalyst used; [c] Residual Pd from synthesis, determined by ICP-OES; [d] Particle size was determined as the Sauter mean diameter by static light scattering in 1:1:1 TEA/MeOH/water; [e] Average transmittance of polymer suspension in 1:1:1 TEA/MeOH/Water; [f] Value obtained from DSA of 3 μL of water dropped onto polymer films drop cast from 1 mg mL⁻¹ solution in chloroform. [g] Due to lack of material polymer rate was measured at a concentration of 1.1 mg mL⁻¹ using 10 mg of photocatalyst, control experiments were run using PS-OTEG and PS-Odec, see Figure S35 and Table S11 (Supporting Information).

However, while the effect of the torsion angle on these oligomers was apparent, it was less pronounced than for P7, PS-ODec, PS-OTEG, and PS-Dodec, as the oligomers reported were, at most, 3 monomer units long and would have possessed naturally shorter conjugation lengths.[26] Also, these oligomers were prepared for

photocatalysis as crystalline/semi-crystalline solids, which would contribute to improved intermolecular interactions.[26]

The difference in photocatalytic performance between PS-ODec and PS-OTEG was relatively simple to understand when considering previous work.[22,35,42–44] Both of these polymers have
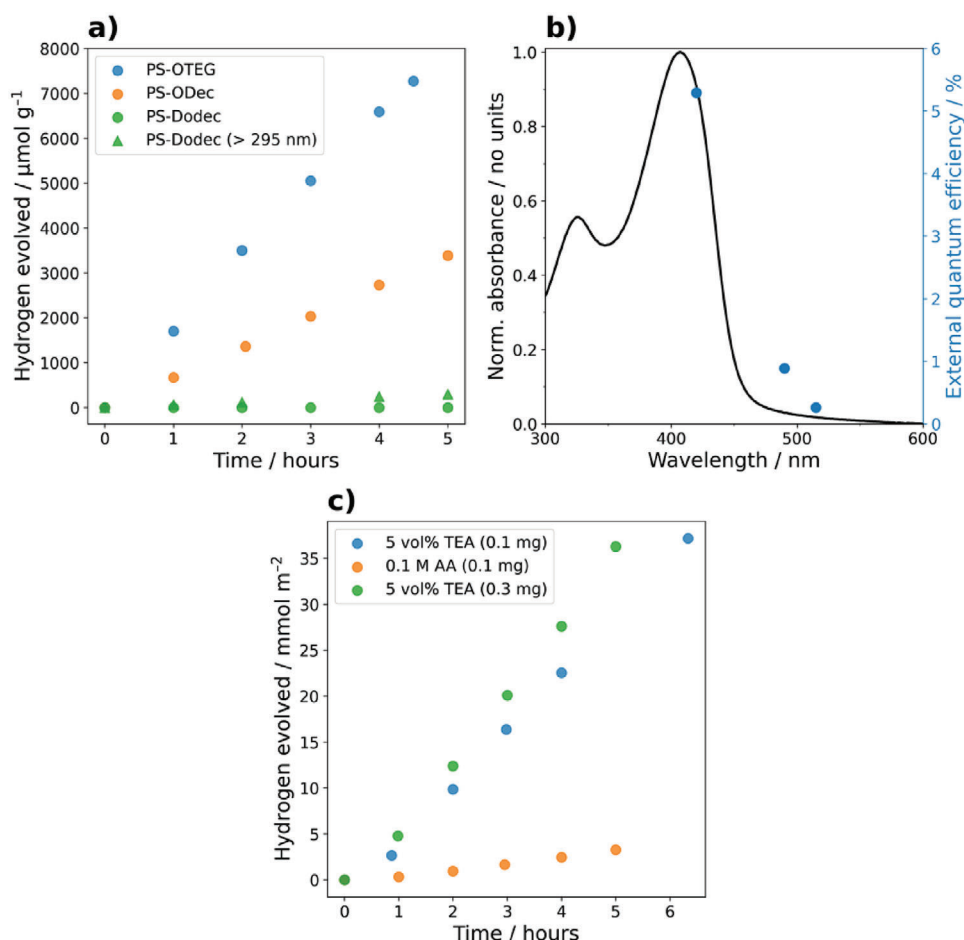

Figure 4. a) Kinetic hydrogen evolution rates of PS-series of polymers as suspensions in 1:1:1 water/MeOH/TEA under visible light illumination (300 W Xe light source, λ > 420 nm filter). B) Plot of the external quantum efficiency of a PS-OTEG suspension in 1:1:1 water/MeOH/TEA superimposed on top of the absorption spectrum of the PS-OTEG thin-film. C) Kinetic hydrogen evolution experiments of thin-films of PS-OTEG on functionalized glass slides in 5 vol% TEA or 0.1 M AA under visible light illumination (300 W Xe light source, λ > 420 nm filter).

ADVANCED
SCIENCE NEWS
www.advancedsciencenews.com

ADVANCED
ENERGY
MATERIALS
www.advenergymat.de

similar opto-electronic properties based on both our empirical and theoretical results (vide supra). Therefore, the difference was likely a consequence of PS-OTEG's superior wettability, dielectric properties, and dispersibility in the reaction mixture (Table 2). The improved wettability can be observed in the significantly lower contact angle seen in the polymer film of PS-OTEG (61.9 ± 0.9°), compared to that of PS-ODec (103.9 ± 2.2°). Under the specified conditions, PS-OTEG was found to disperse better than PS-ODec based on their transmittance data (Table 2), as PS-OTEG only permitted 7% transmittance of light to pass through the suspension, whereas PS-ODec transmitted a much larger 33%. The poorer dispersibility of PS-ODec would contribute to optical losses and an overall reduction in photocatalytic efficiency. Also, since residual palladium acts as a co-catalyst for hydrogen evolution[67] and PS-OTEG had a notably higher residual palladium content than PS-ODec, a potential consequence of chelation of the oligo(ethylene glycol) chains to palladium nanoparticles and, as suggested by Cao and co-workers,[42] it was deemed necessary to briefly study the impact of palladium loading on photocatalytic rate here.[67] We repeated photocatalytic experiments with PS-ODec with higher palladium loadings (full details provided in Figure S32, Supporting Information). However, for the quantities of palladium studied here, it was found that that increasing palladium loading resulted in a reduction, rather than increase, in photocatalytic performance.

Comparing PS-OTEG to P7, we found that our solution processable polymer PS-OTEG could evolve hydrogen at higher rates compared to P7 under similar sacrificial conditions (Table 2). As both PS-OTEG and P7 have similar wettability, palladium contents, and are predicted to have similar levels of backbone torsion, the increased rate is likely a consequence of the narrower optical gap of PS-OTEG, which would allow PS-OTEG to absorb more of the photons delivered by the light source than P7. By contrast, the relatively low rate of PS-ODec versus P7 was likely due to the presence of the hydrophobic side-chains on PS-ODec which will act to minimize the interaction of water with the relatively more hydrophilic conjugated backbone.

2.7. External Quantum Efficiency

The external quantum efficiency (EQE) of PS-OTEG was estimated to be 5.3% at 420 nm for the polymer in a 1:1:1 water/MeOH/TEA suspension. This EQE is comparable to the insoluble analogue, P7, which had an EQE estimated to be 7.2% at 420 nm under the same conditions.[18] However, it is much lower than other insoluble dibenzo[b,d]thiophene sulfone containing polymers reported within our group, such as P38 (a co-polymer of dibenzo[b,d]thiophene sulfone and spirofluorene) and P64 (a co-polymer of dibenzo[b,d]thiophene sulfone and dibenzo[b,d]thiophene) which has EQEs estimated as 18.1%[40] and 20.7%[38] respectively, at 420 nm. However, due to their insolubility in organic solvents for processing, their utility is limited. However, the EQE of PS-OTEG is greater than other solution processable polymers such as PCPDTBSO (a co-polymer of 4,4-bis(2-ethyl-hexyl)−4H-cyclopentadithiophene and dibenzo[b,d]thiophene sulfone), and P8-s (a co-polymer of phenylene and 9-(2-ethylhexyl)−9H-carbazole), which had EQEs

estimated as 0.94%[46] and 0.53%[23] at 420 nm, respectively, as suspensions. However, the EQE of PS-OTEG at 420 nm is lower than PCPDTBSO at longer wavelengths, which had EQEs of 7.8% and 8.7% at the longer wavelengths of 460 nm and 500 nm, respectively.[46] Also, it is significantly lower than the also solution processable fluorene-dibenzo[b,d]thiophene sulfone co-polymer, FS-TEG, which had an EQE of 10% at 420 nm as a suspension in 1:1:1 water/MeOH/TEA, and lower than PCzBPO (a co-polymer of N-phenyl carbazole and 5-phenylbenzo[b]phosphindole-5-oxide), which is reported as having an outstanding EQE of 14.9% at 420 nm.[22,37]

2.8. Stability of Side Chains

A long-term photostability experiment was performed on the second batch of PS-OTEG in a 1:1:1 TEA/MeOH/water suspension (Figure S36, Supporting Information) and as a film in 5 vol% TEA (Figure S56, Supporting Information). For both cases it was found that the hydrogen evolution rate began to decrease within the initial 25 hours and the rate could not be recovered through degassing with nitrogen or upon replacing the water/scavenger mixture (Figure S56, Supporting Information). Analysis of the polymer by UV–vis and $^1H\{^{13}C\}$ NMR spectroscopy (Figures S37 and S38, Supporting Information) showed little change between the as-made material and material post-photocatalysis. Further studies are required to determine whether the stability of the material is compromised under these photocatalytic conditions.[68]

2.9. Photocatalysis of Polymer Thin-Films on Supports

Taking advantage of the solution processability of PS-OTEG, we prepared polymer films by drop-casting dilute solutions of PS-OTEG onto octyl(trichloro)silane (OTS) functionalized glass slides (area = 4.16 cm²). 0.1 mg of PS-OTEG (200 μL of 0.5 mg mL⁻¹) was deposited on the slide to form homogenous films before performing photocatalysis using 0.1 M AA or 5 vol% TEA as sacrificial agents. The 1:1:1 mixture of TEA/MeOH/water used previously for photocatalysts in suspension could potentially result in delamination of PS-OTEG from the substrate, so it was necessary to use the 5 vol.% TEA aqueous solution in place to circumvent this issue. It was found that photocatalysis using 5 vol% TEA resulted in significantly higher hydrogen evolution rates, with a promising area-normalized hydrogen evolution rate of 6.0 ± 0.2 mmol h⁻¹ m⁻² (25.1 mmol h⁻¹ g⁻¹), compared to a relatively poor rate of 0.67 ± 0.04 mmol h⁻¹ m⁻² (2.8 mmol h⁻¹ g⁻¹) when AA was used. The exact reasoning for this almost ninefold increase in rate when the SED is changed from AA to TEA is not fully known and further work would be required to understand the precise reasons. This is, however, consistent with the results of our initial screen of sacrificial conditions, in which TEA (both 5 vol% and 1:1:1 TEA/MeOH/water) outperformed TEOA (10 vol%) and AA (0.1 M) for sacrificial hydrogen evolution (Figure S25, Supporting Information). Recent work by Hillman et al. has suggested that polymers containing the dibenzo[b,d]thiophene sulfone unit are highly

effective at oxidizing TEA, which may partially account for the improved performance of TEA over AA.[69] We then varied the loading of polymer photocatalyst on the support from 0.1 to 0.3 mg (300 μL of 1.0 mg mL^{-1}). However, film inhomogeneity occurred in the form of a "coffee ring" at 0.3 mg polymer loading. Despite numerous attempts to circumvent this issue, we performed photocatalysis with the resultant inhomogeneous film under visible light illumination with a 5 vol.% TEA solution as the sacrificial agent. This film also displayed excellent activity for hydrogen evolution with an area normalized hydrogen evolution rate of 7.4 ± 0.3 mmol h^{-1} m^{-2} (10.2 mmol h^{-1} g^{-1}). Compared to a film of unsubstituted P7, a film of PS-OTEG was found to have approximately twice the mass normalized activity (Figure S57, Supporting Information).

3. Conclusions

In summary, through a combination of calculations and experiment we have demonstrated how minimal variations to side-chain composition can result in drastic changes in the optoelectronic properties and photocatalytic performance of conjugated polymer photocatalysts. We found that functionalizing benzene-dibenzo[*b,d*]thiophene sulfone co-polymers with solubilizing alkyl side-chains, such as *n*-dodecyl (PS-Dodec), can cause significant backbone torsion by virtue of the steric repulsion between the side-chain and hydrogens attached to the adjacent monomer. This increase in torsion of PS-Dodec resulted in a significant blue-shift of the optical gap, relative to its insoluble analogue without side-chains, P7, and a relatively short excited state lifetime. These factors proved to be detrimental to the polymer's photocatalytic performance as no hydrogen was evolved under visible light illumination. We also prepared counter examples in which the alkyl side-chains were substituted for alkoxy side chains, *n*-decoxyl (PS-ODec) and tri(ethylene glycol) (PS-OTEG). In contrast to their alkyl counterparts, the introduction of the alkoxy side chains was associated with reduced torsion of the backbone due to the formation of intramolecular non-conventional hydrogen bonds and reduced steric repulsion. Our DFT calculations suggested that the torsion angle of our soluble alkoxy polymers would approach the torsion angle predicted for the insoluble side-chain-less P7. The alkoxy side-chains were also found to further influence the polymers through mesomeric donation by the electron rich oxygen into the polymer backbone. This mesomeric donation resulted in improved donor character of the phenylene-type monomer and narrowing of the optical gap, as predicted both in our calculations and observed experimentally from the polymer's measured UV–Vis spectra. Both PS-ODec and PS-OTEG showed promising hydrogen evolution rates of 17.0 and 45.4 μmol h^{-1}, respectively, as suspension in a water/triethylamine/methanol mixture when irradiated by visible light, with the activity of the latter exceeding that of the insoluble P7 under the same conditions. The most active of the polymers, PS-OTEG, was estimated to have an EQE of 5.3% at 420 nm in suspension. We finally demonstrated an advantage of the solubility of PS-OTEG by fabricating a simple thin-film photocatalyst on a glass support. This thin-film photocatalyst demonstrated an encouraging area-normalized sacrificial hydrogen evolution rate of 7.35 mmol h^{-1} m^{-2} under visible light irradiation.

Conflict of Interest

The authors declare no conflict of interest.

Data Availability Statement

The data that support the findings of this study are available in the supplementary material of this article.

[1] Y. Wang, A. Vogel, M. Sachs, R. S. Sprick, L. Wilbraham, S. J. A. Moniz, R. Godin, M. A. Zwijnenburg, J. R. Durrant, A. I. Cooper, J. Tang, *Nat. Energy* **2019**, *4*, 746.

[2] J. Jayakumar, H. H. Chou, *ChemCatChem* **2020**, *12*, 689.

[3] A. Fujishima, K. Honda, *Nature* **1972**, *238*, 37.

[4] Z. Wang, C. Li, K. Domen, *Chem. Soc. Rev.* **2019**, *48*, 2109.

[5] Q. Wang, K. Domen, *Chem. Rev.* **2020**, *120*, 919.

[6] K. Maeda, K. Domen, *J. Phys. Chem. Lett.* **2010**, *1*, 2655.

[7] S. Yanagida, A. Kabumoto, K. Mizumoto, C. Pac, K. Yoshino, *J. Chem. Soc., Chem. Commun.* **1985**, *0*, 474.

[8] X. Wang, K. Maeda, X. Chen, K. Takanabe, K. Domen, Y. Hou, X. Fu, M. Antonietti, *J. Am. Chem. Soc.* **2009**, *131*, 1680.

[9] X. Wang, K. Maeda, A. Thomas, K. Takanabe, G. Xin, J. M. Carlsson, K. Domen, M. Antonietti, *Nat. Mater.* **2009**, *8*, 76.

[10] C. B. Meier, R. Clowes, E. Berardo, K. E. Jelfs, M. A. Zwijnenburg, R. S. Sprick, A. I. Cooper, *Chem. Mater.* **2019**, *31*, 8830.

[11] C. B. Meier, R. S. Sprick, A. Monti, P. Guiglion, J.-S. M. Lee, M. A. Zwijnenburg, A. I. Cooper, *Polymer* **2017**, *126*, 283.

[12] J. Wang, G. Ouyang, Y. Wang, X. Qiao, W. S. Li, H. Li, *Chem. Commun.* **2020**, *56*, 1601.

[13] J. M. Lee, A. I. Cooper, *Chem. Rev.* **2020**, *120*, 2171.

[14] L. Stegbauer, K. Schwinghammer, B. V. Lotsch, *Chem. Sci.* **2014**, *5*, 2789.

[15] V. S. Vyas, F. Haase, L. Stegbauer, G. Savasci, F. Podjaski, C. Ochsenfeld, B. V. Lotsch, *Nat. Commun.* **2015**, *6*, 8508.

[16] X. Wang, L. Chen, S. Y. Chong, M. A. Little, Y. Wu, W. H. Zhu, R. Clowes, Y. Yan, M. A. Zwijnenburg, R. S. Sprick, A. I. Cooper, *Nat. Chem.* **2018**, *10*, 1180.

**ADVANCED
SCIENCE NEWS**

www.advancedsciencenews.com

**ADVANCED
ENERGY
MATERIALS**

www.advenergymat.de

[17] W. Zhang, L. Chen, S. Dai, C. Zhao, C. Ma, L. Wei, M. Zhu, S. Y. Chong, H. Yang, L. Liu, Y. Bai, M. Yu, Y. Xu, X. W. Zhu, Q. Zhu, S. An, R. S. Sprick, M. A. Little, X. Wu, S. Jiang, Y. Wu, Y. B. Zhang, H. Tian, W. H. Zhu, A. I. Cooper, *Nature* **2022**, *604*, 72.

[18] M. Sachs, R. S. Sprick, D. Pearce, S. A. J. Hillman, A. Monti, A. A. Y. Guilbert, N. J. Brownbill, S. Dimitrov, X. Shi, F. Blanc, M. A. Zwijnenburg, J. Nelson, J. R. Durrant, A. I. Cooper, *Nat. Commun.* **2018**, *9*, 4968.

[19] R. S. Sprick, B. Bonillo, R. Clowes, P. Guiglion, N. J. Brownbill, B. J. Slater, F. Blanc, M. A. Zwijnenburg, D. J. Adams, A. I. Cooper, *Angew. Chem.* **2016**, *128*, 1824.

[20] R. S. Sprick, L. Wilbraham, Y. Bai, P. Guiglion, A. Monti, R. Clowes, A. I. Cooper, M. A. Zwijnenburg, *Chem. Mater.* **2018**, *30*, 5733.

[21] A. Vogel, M. Forster, L. Wilbraham, C. L. Smith, A. J. Cowan, M. A. Zwijnenburg, R. S. Sprick, A. I. Cooper, *Faraday Discuss.* **2019**, *215*, 84.

[22] D. J. Woods, S. A. J. Hillman, D. Pearce, L. Wilbraham, L. Q. Flagg, W. Duffy, I. McCulloch, J. R. Durrant, A. A. Y. Guilbert, M. A. Zwijnenburg, R. S. Sprick, J. Nelson, A. I. Cooper, *Energy Environ. Sci.* **2020**, *13*, 1843.

[23] D. J. Woods, R. S. Sprick, C. L. Smith, A. J. Cowan, A. I. Cooper, *Adv. Energy Mater.* **2017**, *7*, 1700479.

[24] P. Verma, A. Singh, F. A. Rahimi, P. Sarkar, S. Nath, S. K. Pati, T. K. Maji, *Nat. Commun.* **2021**, *12*, 7313.

[25] C. M. Aitchison, C. M. Kane, D. P. McMahon, P. R. Spackman, A. Pulido, X. Wang, L. Wilbraham, L. Chen, R. Clowes, M. A. Zwijnenburg, R. S. Sprick, M. A. Little, G. M. Day, A. I. Cooper, *J. Mater. Chem. A* **2020**, *8*, 7158.

[26] C. M. Aitchison, M. Sachs, M. A. Little, L. Wilbraham, N. J. Brownbill, C. M. Kane, F. Blanc, M. A. Zwijnenburg, J. R. Durrant, R. S. Sprick, A. I. Cooper, *Chem. Sci.* **2020**, *11*, 8744.

[27] X. Li, P. M. Maffettone, Y. Che, T. Liu, L. Chen, A. I. Cooper, *Chem. Sci.* **2021**, *12*, 10742.

[28] Z. Zhang, W. Si, B. Wu, W. Wang, Y. Li, W. Ma, Y. Lin, *Angew. Chem., Int. Ed.* **2022**, *61*, 202114234.

[29] Y. Zhu, Z. Zhang, W. Si, Q. Sun, G. Cai, Y. Li, Y. Jia, X. Lu, W. Xu, S. Zhang, Y. Lin, *J. Am. Chem. Soc.* **2022**, *144*, 12747.

[30] H. Yang, C. Li, T. Liu, T. Fellowes, S. Y. Chong, L. Catalano, M. Bahri, W. Zhang, Y. Xu, L. Liu, W. Zhao, A. M. Gardner, R. Clowes, N. D. Browning, X. Li, A. J. Cowan, A. I. Cooper, *Nat. Nanotechnol.* **2023**, *18*, 307.

[31] A. Liu, C.-W. Tai, K. Holá, H. Tian, *J. Mater. Chem. A* **2019**, *7*, 4797.

[32] P.-J. Tseng, C.-L. Chang, Y.-H. Chan, L.-Y. Ting, P.-Y. Chen, C.-H. Liao, M.-L. Tsai, H.-H. Chou, *ACS Catal.* **2018**, *8*, 7766.

[33] L. Wang, R. Fernandez-Teran, L. Zhang, D. L. Fernandes, L. Tian, H. Chen, H. Tian, *Angew. Chem., Int. Ed.* **2016**, *55*, 12306.

[34] Y. Gwon, Y. Jo, H.-J. Lee, S. Y. Park, T. S. Lee, *Polymer* **2021**, *229*, 124004.

[35] M. Yu, W. Zhang, Z. Guo, Y. Wu, W. Zhu, *Angew. Chem., Int. Ed.* **2021**, *60*, 15590.

[36] R. S. Sprick, K. J. Cheetham, Y. Bai, J. Alves Fernandes, M. Barnes, J. W. Bradley, A. I. Cooper, *J. Mater. Chem. A* **2020**, *8*, 7125.

[37] W.-H. Wang, L.-Y. Ting, J. Jayakumar, C.-L. Chang, W.-C. Lin, C.-C. Chung, M. H. Elsayed, C.-Y. Lu, A. M. Elewa, H.-H. Chou, *Sustainable Energy Fuels* **2020**, *4*, 5264.

[38] Y. Bai, L. Wilbraham, B. J. Slater, M. A. Zwijnenburg, R. S. Sprick, A. I. Cooper, *J. Am. Chem. Soc.* **2019**, *141*, 9063.

[39] Z. R. Tan, Y. Q. Xing, J. Z. Cheng, G. Zhang, Z. Q. Shen, Y. J. Zhang, G. Liao, L. Chen, S. Y. Liu, *Chem. Sci.* **2022**, *13*, 1725.

[40] Y. Bai, L. Wilbraham, H. Gao, R. Clowes, H. Yang, M. A. Zwijnenburg, A. I. Cooper, R. S. Sprick, *J. Mater. Chem. A* **2021**, *9*, 19958.

[41] C. Han, S. Xiang, S. Jin, L.-W. Luo, C. Zhang, C. Yan, J.-X. Jiang, *J. Mater. Chem. A* **2022**, *10*, 5255.

[42] Z. Hu, Z. Wang, X. Zhang, H. Tang, X. Liu, F. Huang, Y. Cao, *iScience* **2019**, *13*, 33.

[43] J. Kosco, S. Gonzalez-Carrero, C. T. Howells, W. Zhang, M. Moser, R. Sheelamanthula, L. Zhao, B. Willner, T. C. Hidalgo, H. Faber, B. Purushothaman, M. Sachs, H. Cha, R. Sougrat, T. D. Anthopoulos, S. Inal, J. R. Durrant, I. McCulloch, *Adv. Mater.* **2021**, *34*, 2105007.

[44] R. Diao, H. Ye, Z. Yang, S. Zhang, K. Kong, J. Hua, *Polym. Chem.* **2019**, *10*, 6473.

[45] F. Y. Cao, C. L. Huang, T. Y. Cheng, H. J. Cheng, T. K. Wu, Y. J. Cheng, *ACS Macro Lett.* **2023**, *12*, 468.

[46] W.-C. Lin, J. Jayakumar, C.-L. Chang, L.-Y. Ting, M. H. Elsayed, M. Abdellah, K. Zheng, A. M. Elewa, Y.-T. Lin, J.-J. Liu, W.-S. Wang, C.-Y. Lu, H.-H. Chou, *Appl. Catal., B* **2021**, *298*, 120577.

[47] Y. Bai, D. J. Woods, L. Wilbraham, C. M. Aitchison, M. A. Zwijnenburg, R. S. Sprick, A. I. Cooper, *J. Mater. Chem. A* **2020**, *8*, 8700.

[48] Y. Che, D. F. Perepichka, *Angew. Chem., Int. Ed.* **2021**, *60*, 1364.

[49] Z. A. Lan, M. Wu, Z. Fang, X. Chi, X. Chen, Y. Zhang, X. Wang, *Angew. Chem., Int. Ed.* **2021**, *60*, 16355.

[50] P. Pracht, F. Bohle, S. Grimme, *Phys. Chem. Chem. Phys.* **2020**, *22*, 7169.

[51] A. D. Becke, *J. Chem. Phys.* **1993**, *98*, 5648.

[52] C. Lee, W. Yang, R. G. Parr, *Phys. Rev. B* **1988**, *37*, 785.

[53] S. H. Vosko, L. Wilk, M. Nusair, *Can. J. Phys.* **1980**, *58*, 1200.

[54] P. J. Stephens, F. J. Devlin, C. F. Chabalowski, M. J. Frisch, *J. Phys. Chem.* **1994**, *98*, 11623.

[55] E. Caldeweyher, C. Bannwarth, S. Grimme, *J. Chem. Phys.* **2017**, *147*, 034112.

[56] P. Guiglion, C. Butchosa, M. A. Zwijnenburg, *J. Mater. Chem. A* **2014**, *2*, 11996.

[57] P. Guiglion, A. Monti, M. A. Zwijnenburg, *J. Phys. Chem. C* **2017**, *121*, 1498.

[58] A. Bondi, *J. Phys. Chem.* **1964**, *68*, 441.

[59] I. A. Wright, H. A. Al-Attar, A. S. Batsanov, A. P. Monkman, M. R. Bryce, *Phys. Chem. Chem. Phys.* **2018**, *20*, 11867.

[60] C. J. Mueller, E. Gann, C. R. Singh, M. Thelakkat, C. R. McNeill, *Chem. Mater.* **2016**, *28*, 7088.

[61] Z. D. Yu, Y. Lu, J. Y. Wang, J. Pei, *Chemi. Eur. J.* **2020**, *26*, 16194.

[62] D. L. Meyer, N. Schmidt-Meinzer, C. Matt, S. Rein, F. Lombeck, M. Sommer, T. Biskup, *J. Phys. Chem. C* **2019**, *123*, 20071.

[63] B. Meng, H. Song, X. Chen, Z. Xie, J. Liu, L. Wang, *Macromolecules* **2015**, *48*, 4357.

[64] S. Moro, N. Siemons, O. Drury, D. A. Warr, T. A. Moriarty, L. M. A. Perdigao, D. Pearce, M. Moser, R. K. Hallani, J. Parker, I. McCulloch, J. M. Frost, J. Nelson, G. Costantini, *ACS Nano* **2022**, *16*, 21303.

[65] R. S. Sprick, B. Bonillo, M. Sachs, R. Clowes, J. R. Durrant, D. J. Adams, A. I. Cooper, *Chem. Commun.* **2016**, *52*, 10008.

[66] Z. A. Lan, G. Zhang, X. Chen, Y. Zhang, K. A. I. Zhang, X. Wang, *Angew. Chem., Int. Ed.* **2019**, *58*, 10236.

[67] J. Kosco, M. Sachs, R. Godin, M. Kirkus, L. Francas, M. Bidwell, M. Qureshi, D. Anjum, J. R. Durrant, I. McCulloch, *Adv. Energy Mater.* **2018**, *8*, 1802181.

[68] T. Yabuta, M. Hayashi, R. Matsubara, *J. Org. Chem.* **2021**, *86*, 2545.

[69] S. A. J. Hillman, R. S. Sprick, D. Pearce, D. J. Woods, W. Y. Sit, X. Shi, A. I. Cooper, J. R. Durrant, J. Nelson, *J. Am. Chem. Soc.* **2022**, *144*, 19382.